Electronic structure and positron states at vacancies in Si and GaAs

M. J. Puska,* O. Jepsen, and O. Gunnarsson
Max-Planck-Institut für Festkörperforschung, D-7000 Stuttgart 80, Federal Republic of Germany

R. M. Nieminen
Department of Physics, University of Jyväskylä, SF-40100 Jyväskylä, Finland
(Received 16 January 1986)

The self-consistent electron structures of the perfect Si and GaAs lattices are calculated by the linear-muffin-tin-orbital (LMTO) band-structure method within the atomic-sphere approximation (ASA). Monovacancies in different charge states are treated by the self-consistent LMTO-ASA Green's-function method. The corresponding positron states are determined by the same methods and positron annihilation characteristics are calculated. The results are compared with recent experiments.

I. INTRODUCTION

Although there exist several experimental methods (e.g., optical, transient capacitance, electron-spin-resonance, etc.) for measuring defect-induced properties in semiconductors, the identification of the different types of defects, especially in compound semiconductors, is still on a rather unsatisfactory level.[1,2] Recently, the positron annihilation technique,[3] long established as a major tool for studying atomic defects in metals,[4] has emerged as a potentially powerful tool for identification of point defects in semiconductors.[5–8] However, the interpretation of, e.g., positron lifetime data is made difficult by ambiguities. For example, certain lifetime components corresponding to trapped positrons in GaAs are associated with different types of defects in different works[5,6] and there is an appreciable scatter even in the extracted positron lifetimes for the perfect crystal. The reason for these difficulties lies in the large number of different defects (vacancies, self-interstitials, impurities, antisites, and complexes of them) which can in addition exist in several charge states. The lack of reliable calculations for positron states and predictions for annihilation characteristics at different defects has hampered an understanding. This paper is meant to remedy the need for theoretical work by representing results from detailed calculations of electronic structure, positron states, and annihilation characteristics in perfect Si and GaAs and at monovacancies in these crystals.

The positron lifetime technique is a well-established method for monitoring the development of vacancy-type defects (i.e., vacancies, vacancy clusters, vacancy-impurity complexes).[3,4] These defects can trap a positron and, due to the change of the electronic environment, the positron lifetime changes from the perfect lattice value. For the interpretation of the experimental results a comparison with theoretical calculations has turned out to be very fruitful.[9–13] In order to calculate the positron wave-function and annihilation characteristics, the electronic structure of the perfect and defected lattice is needed. In metals the simple construction of the charge density by superposition of free atomic densities is a reasonable first approximation in an efficient and practical calculational method,[9] in which the positron wave function is calculated for the full three-dimensional potential. The potential can be constructed from the charge densities of the host metal (and possible impurity) atoms, placed at appropriate positrons. The non-self-consistency of the electron density has been found to play a minor role in the determination of the positron lifetime. This is because the lifetime is related to an overlap integral of the positron and electron densities: when the electron density relaxes towards self-consistency the positron density follows, so that the change in the overlap is small. On the other hand, the positron energy eigenvalue can be rather sensitive to the detailed shape of the electronic density.

In *covalent semiconductors* with directed bonds the electronic density constructed by superposing atomic densities is doubtful, especially for a reliable estimation of positron energy levels. In this work we use the linear-muffin-tin-orbital method (LMTO) to calculate the self-consistent electronic structures.[14–16] The atomic-sphere approximation (ASA) is used, i.e., potentials and charge densities are spherical averages within spheres, centered both at host nuclei and (in semiconductors) at interstitial sites. The spheres overlap and fill up the whole lattice space. The electron structure is calculated self-consistently within the local-density approximation for electronic exchange and correlation. The electronic structure of the *perturbed crystal* is calculated by the LMTO Green's-function method,[17] in which one or several perfect-lattice atoms are substituted by defect atoms and the resulting electronic structure is calculated self-consistently inside a region around the defects and their nearest neighbors. The same methods are used to calculate positron states. In the present calculations the ASA is used both for the perfect crystal and for the defected one. The geometry violation due to the ASA in the interstitial region is not severe for the electron states,[18] and this holds also for the positron states as discussed below. More important, especially for the energetics, is that the electron charge density is determined self-consistently.

The LMTO-ASA method has previously been used for the calculation of positron states in bulk metals by Singh and Jarlborg.[19] They showed that the ASA describes well the momentum distribution of the annihilating electron-positron pair in the first Brillouin zone. For the Umklapp processes a simple correction beyond the ASA is needed.

The LMTO-ASA Green's-function method has previously been successfully applied in predicting the properties of chalcogen[20] and transition-metal[21] impurities in silicon. In this paper we present results of LMTO-ASA Green's-function calculations for vacancies in Si and GaAs. In the calculations the ions around the vacancies are not allowed to relax from their perfect-lattice positrons, i.e., calculations are made for "ideal" vacancies. In Sec. II we briefly describe the LMTO-ASA method and the corresponding Green's-function method. Moreover, in Sec. II the construction of the positron potential and the calculation of the positron lifetime are discussed. The resulting electronic structures of the vacancy defects are described rather carefully in the beginning of Sec. III, in order to understand the response of positrons to vacancies in semiconductors. Thereafter, the results for the positron annihilation characteristics at vacancies in Si and GaAs are presented and compared with experimental results. In Sec. IV we summarize our results.

II. THEORY

A. Electronic structure calculations

The LMTO method for self-consistent calculation of the electronic structure of perfect crystals, as well as its Green's-function extension to treat defects in solids, have been discussed in detail in Refs. 14 to 17. We shall therefore comment only on those aspects which are particularly relevant to this calculation.

In the LMTO method[14–16] the crystal space is divided into spheres and an interstitial region and in the ASA the spheres are expanded so that they fill the space. In the case of close-packed structures all spheres are centered around atomic nuclei and the radius of the spheres is equal to the Wigner-Seitz radius. For the semiconductors with diamond or zinc-blende structures considered in this work, half of the spheres are centered at nuclei and half at interstitial sites.

The valence electron density $n(\mathbf{r})$ is calculated, in accordance with the density-functional theory, as a sum over occupied single-particle states belonging to the valence bands:

$$n(\mathbf{r})=\sum_{j}^{\text{occ}} |\psi_j(\mathbf{r})|^2 . \tag{1}$$

For the core electrons, frozen atomic orbitals are used. In the LMTO-ASA method the wave functions ψ_j may be expressed as one-center expansions:

$$\psi_j(\mathbf{r})=\sum_{\mathbf{R},L}\phi_{\mathbf{R}L}(E,\mathbf{r}_\mathbf{R})u_{\mathbf{R}L,j} , \tag{2}$$

where $\mathbf{r}_\mathbf{R}=\mathbf{r}-\mathbf{R}$, L is a compact notation for angular momentum quantum numbers l and m, $\phi_{\mathbf{R}L}(E,\mathbf{r}_\mathbf{R})$ is the solution of the scalar relativistic Schrödinger equation at energy E, and $u_{\mathbf{R}L,j}$ are the eigenvectors. In the LMTO method the basis function ϕ's are linearized around the fixed but arbitrary energy $E_{\nu\mathbf{R}l}$

$$\phi_{\mathbf{R}L}(E,\mathbf{r}_\mathbf{R})=\phi_{\mathbf{R}L}(E_{\nu\mathbf{R}l},\mathbf{r}_\mathbf{R})+\dot{\phi}_{\mathbf{R}L}(E_{\nu\mathbf{R}l},\mathbf{r}_\mathbf{R})(E-E_{\nu\mathbf{R}l}) , \tag{3}$$

where the dot denotes the derivative with respect to energy. $\phi_{\mathbf{R}L}$ and $\dot{\phi}_{\mathbf{R}L}$ are orthogonal and they vanish outside the sphere centered at the site $\mathbf{R}$ by definition.

The exact (not linearized) wave functions may on the other hand also be expressed as a multicenter expansion of energy-dependent functions, the so-called muffin-tin orbitals (χ^α), which extend over all space:

$$\psi_j(E,\mathbf{r})=\sum_{\mathbf{R}L}\chi^\alpha_{\mathbf{R}L}(E,\mathbf{r}_\mathbf{R})u_{\mathbf{R}L,j}(E) . \tag{4}$$

In the ASA, where the interstitial region is neglected, χ^α has the form[16]

$$\chi^\alpha_{\mathbf{R}L}(E,\mathbf{r}_\mathbf{R})=\phi_{\mathbf{R}L}(E,\mathbf{r}_\mathbf{R})+\sum_{\mathbf{R}',L'}\dot{\phi}^\alpha_{\mathbf{R}'L'}(E,\mathbf{r}_{\mathbf{R}'})h^\alpha_{\mathbf{R}'L',\mathbf{R}L}(E) , \tag{5}$$

where $\dot{\phi}^\alpha$ is a linear combination of the orthogonal ϕ and $\dot{\phi}$ corresponding to a certain set (α) of muffin-tin orbitals obtained by using a certain multipole field as an envelope function.[16,22] In (5) the expansion matrix $h^\alpha(E)$ has the form[16]

$$h^\alpha(E)=[\dot{P}^\alpha(E)]^{-1/2}[-P^\alpha(E)+S^\alpha][\dot{P}^\alpha(E)]^{-1/2} . \tag{6}$$

Above, P^α, the so-called potential function, is a diagonal matrix which depends on the potential inside the sphere at $\mathbf{R}$ via the logarithmic derivative at the sphere radius, but not on the atomic positions. The information about the atomic positions is contained in the structure constant matrix S^α. It depends on the chosen muffin-tin-orbital (MTO) representation α but not on the potential or the scale of the structure. S^α can be expressed in terms of the familiar canonical structure constant matrix S^0 as[16,22]

$$S^\alpha=S^0(1-\alpha S^0)^{-1} . \tag{7}$$

Here, α is a diagonal matrix determining the MTO representation.

Inserting Eqs. (6) and (7) into Eq. (5) we obtain the following multicenter expansion:

$$\psi_j(E,\mathbf{r})=\sum_{\mathbf{R},L}\phi_{\mathbf{R}L}(E,\mathbf{r}_\mathbf{R})u_{\mathbf{R}L,j}(E) + \sum_{\mathbf{R},L}\sum_{\mathbf{R}',L'}\dot{\phi}^\alpha_{\mathbf{R}'L'}(E,\mathbf{r}_{\mathbf{R}'})[\dot{P}^\alpha_{\mathbf{R}'L'}(E)]^{-1/2}[-P^\alpha_{\mathbf{R}'L'}(E)\delta_{\mathbf{R},\mathbf{R}'}\delta_{LL'}+S^\alpha_{\mathbf{R}'L',\mathbf{R}L}][\dot{P}^\alpha_{\mathbf{R}L}(E)]^{-1/2}u_{\mathbf{R}L,j}(E) . \tag{8}$$

This expression is equivalent to the one-center expansion (2) if the second term on the right-hand side vanishes. This condition gives the Korringa-Kohn-Rostoker equations

$$\sum_{\mathbf{R},L}[-P^{\alpha}_{\mathbf{R}'L'}(E)\delta_{\mathbf{R}\mathbf{R}'}\delta_{LL'}+S^{\alpha}_{\mathbf{R}'L',\mathbf{R}L}]\times[\dot{P}^{\alpha}_{\mathbf{R}L}(E)]^{-1/2}u_{\mathbf{R}L,j}(E)=0\ , \quad (9)$$

in the ASA, if the potential function is calculated exactly for every energy. In the linearized method the following parametrization is used for the potential function

$$P^{\alpha}_{\mathbf{R}L}(E)=\frac{E-C_{\mathbf{R}l}}{(E-C_{\mathbf{R}l})(\gamma_{\mathbf{R}l}-\alpha_{\mathbf{R}l})+\Delta_{\mathbf{R}l}}\ , \quad (10)$$

where $C_{\mathbf{R}l}$, $\Delta_{\mathbf{R}l}$, and $\gamma_{\mathbf{R}l}$ are potential parameters and $\alpha_{\mathbf{R}l}$ is the above-mentioned matrix determining the MTO representation. The potential parameters are determined at the energy $E_{\nu\mathbf{R}l}$ and depend on the potential inside the sphere $\mathbf{R}$ but not on the lattice structure. Using this parametrization the tail-cancellation condition reduces to an eigenvalue problem.

For a perfect crystal we use the Bloch symmetry and solve for the energy eigenvalues $E_j(\mathbf{k})$ and the eigenvectors $u_{\mathbf{T}L,j}(\mathbf{k})$, where $\mathbf{k}$ is the Bloch vector and $\mathbf{T}$ labels the atom in the unit cell. The eigenvectors are then used in a one-center expansion similar to (2) in order to calculate the spherical charge densities.

For the *defect* calculations, the perfect-lattice Green's function has first to be constructed. The effective Hamiltonian corresponding to the secular equation (9) reads as[17] (in the following we drop the indices $\mathbf{R}$ and L)

$$H_0^{\gamma_0}=C_0+\Delta_0^{1/2}S^{\gamma_0}\Delta_0^{1/2}\ , \quad (11)$$

where we have chosen $\alpha=\gamma$, because this MTO representation is used to calculate the band structure. The subscript 0 refers to the unperturbed system. The corresponding Green's function is defined formally as

$$G_0^{\gamma_0}(E)=(E-i0^+-H_0^{\gamma_0})^{-1}\ . \quad (12)$$

The imaginary part of the Green's function is proportional to the unperturbed projected density of states (DOS), i.e.,

$$\mathrm{Im}G_0^{\gamma_0}(E)=\pi N_0^{\gamma_0}(E)\ , \quad (13)$$

and the complete Green's function can be calculated in a general point z of the complex energy plane by the Hilbert transform

$$G_0^{\gamma_0}(z)=\int_{-\infty}^{\infty}\frac{N_0^{\gamma_0}(E')}{z-E'}dE'\ . \quad (14)$$

In practice, we calculate the Hilbert transform using the projected integrated DOS, $n_0^{\gamma_0}(E)$, so that

$$G_0^{\gamma_0}(z)=\frac{n_0^{\gamma_0}(E_2)}{z-E_2}-\int_{E_1}^{E_2}\frac{n_0^{\gamma_0}(E')}{(z-E')^2}dE'\ , \quad (15)$$

where E_1 and E_2 are the bottom of the lowest LMTO band and the top of the highest LMTO band, respectively. In the LMTO Green's-function method, contrary to many other Green's-function methods, there is a natural cutoff for the energy integral in the Hilbert transform. The use of the integrated DOS instead of the DOS reduces considerably the number of energy points needed in the Hilbert transform. The projected integrated DOS is calculated using the tetrahedron method[23] as [17]

$$n^{\gamma_0}_{0\mathbf{T}'L',(\mathbf{T}+\mathbf{R})L}(E)=(V_{\mathrm{BZ}})^{-1}\int_{E_1}^{E}dE'\sum_{j}^{\text{bands}}\int_{V_{\mathrm{BZ}}}d^3k\,\exp(i\mathbf{k}\cdot\mathbf{R})u^{*}_{\mathbf{T}'L',j}(\mathbf{k})u_{\mathbf{T}L,j}(\mathbf{k})\delta(E-E_j(\mathbf{k}))\ , \quad (16)$$

where $\mathbf{R}$ is a Bravais-lattice vector and V_{BZ} is the volume of the Brillouin zone.

Instead of using $G_0^{\gamma_0}$ as the starting point in the Dyson's equation for the defect problem, it is more convenient to use the Green's-function matrix g_0^{α} corresponding directly to the secular equation (9). The matrix g_0 is defined as[17]

$$g_0^{\alpha}(E)=(P_0^{\alpha}-i0^+-S^{\alpha})^{-1}\ , \quad (17)$$

where 0 denotes the unperturbed system and α refers to a chosen MTO representation.[22] The Green's function g^{α} is related to G^{γ} defined above by the transformations[22]

$$g^{\gamma}(E)=\Delta^{1/2}G^{\gamma}(E)\Delta^{1/2}\ , \quad (18)$$

$$g^{\alpha}(E)=(\alpha-\gamma)\frac{P^{\gamma}(E)}{P^{\alpha}(E)}+\frac{P^{\gamma}(E)}{P^{\alpha}(E)}g^{\gamma}(E)\frac{P^{\gamma}(E)}{P^{\alpha}(E)}\ . \quad (19)$$

These equations hold for the unperturbed system as well as for the perturbed one. Moreover, Eq. (19) gives the general transformation between any two MTO representations.

The Green's function for the perturbed system is obtained by solving the Dyson's equation[17]

$$\{1+g_0^{\alpha}(E)[P^{\alpha}(E)-P_0^{\alpha}(E)]\}g^{\alpha}(E)=g_0^{\alpha}(E)\ , \quad (20)$$

which is essentially a finite set of linear equations. The Dyson's equation for the perturbed Green's function g^{α} is used instead of the Dyson's equation for the Hamiltonian Green's function G^{α}, because the perturbation is then more localized. Furthermore, it is diagonal in $\mathbf{R}$ and L.

The Dyson's equation is solved iteratively. In the first iteration the perturbation $\Delta P^{\alpha}(E)$ is determined from a starting potential, the perturbed electron density is calculated, and the potential for the next iteration is obtained in the local-density approximation. In the actual calculations the Dyson's equation (20) is solved in the $\alpha=\gamma^i$ representation, where $\gamma_{\mathbf{R}l}$ are the potential parameters corresponding to the potential of the ith iteration. In this way numerical inaccuracies due to the poles of $\dot{P}^{\alpha}$ are avoided,

since the transformation (18) takes this simple form only in the γ representation. The perturbed Green's function is then transformed back to g^{γ} via (19) and G^{γ} is obtained from (18). The calculation of the electron density is performed by integrating $G^{\gamma}(E)$ along a rectangular path in the complex energy plane. This path starts on the real axis below the valence bands and it ends on the real axis at the top of the valence band or at the Fermi level for semiconductors and metals, respectively. The deformation of the integration path from the real axis into the complex plane smooths the structure in the Green's function and makes an accurate density calculation with few energy points possible.[24]

The positions of the bound states are determined by searching for the solutions of the equation

$$\det[1+g_0^{\gamma_i}(E)\Delta P^{\gamma_i}]=0 \quad (21).$$

below the valence bands and in the band gaps. The contribution to the electron density from bound states below the valence bands is taken into account by starting the complex energy path on the real axis below the lowest bound states. For the bound states within a band gap a separate complex path is introduced to allow for a different occupancy of these.

The unperturbed Green's function is correct to second order in $E-E_v$. In order to improve the description in the perturbed region we have used the following third-order parametrization for the potential function

$$P_{\mathbf{R}l}^{(3)\alpha}(E)=P_{\mathbf{R}}^{(2)\alpha}(E+p_{\mathbf{R}l}(E-E_{v\mathbf{R}l})^3) , \quad (22)$$

where $p_{Rl}=\int_0^{s_{\mathbf{R}}}(\dot{\phi}_{\mathbf{R}l}(r))^2r^2dr$ and $P^{(2)\alpha}(E)$ is the second-order function (10).

B. Calculation of positron states

The complete solution of the problem of a localized positron interacting with the electrons around a defect requires the simultaneous self-consistent calculation of the electronic structure and the positron state. This is possible in the two-component density-functional theory,[25–29] but the application of the theory beyond simple model systems such as the jellium vacancy[28,29] is very time-consuming. We therefore follow the conventional route and first solve for the electron structure problem without the positron present. Thereafter the positron state is calculated modeling the electron-positron correlation by an electron-density-dependent correlation term in the positron potential. The model calculations[28,29] employing the full two-component theory have shown that this approximation is a good one, in particular, for the positron lifetime, which is central in defect spectroscopy.

We have used the same techniques (described in Sec. II A) for the positron calculations as for the electron-state calculations. After the electron density is known, the potential sensed by the positron in all space is constructed as

$$V^{+}(\mathbf{r})=V_{\text{Coulomb}}(\mathbf{r})+V_{\text{corr}}(n(\mathbf{r})) , \quad (23)$$

where V_{Coulomb} is the electronic Hartree (Coulomb) potential and V_{corr} is the correlation potential, which describes the effects due to the short-range pileup of electrons near the positron. We treat V_{corr} in the local-density approximation and use the parametrization

$$V_{\text{corr}}(n)=V_{\text{corr}}^{eg}(n)[f(n,\varepsilon_g)]^{1/3} , \quad (24)$$

where $V_{\text{corr}}^{eg}(n)$ is the correlation energy for a positron in a homogeneous electron gas with density n.[30] In Eq. (24), $f(n,\varepsilon_g)$ is a reduction factor, which accounts for the diminished response (screening) of semiconductors to charged particles, in comparison with (simple) metals where $f=1$. This has been discussed by Brandt and Reinheimer,[31] and we use the following interpolation formula to fit their numerical data, obtained from screening calculations for point charges in a model semiconductor:

$$f(n,\varepsilon_g)=1-\frac{0.37\varepsilon_g}{1+0.18r_s}, \quad r_s=\left[\frac{3}{4\pi n}\right]^{1/3} . \quad (25)$$

Above, ε_g is a "gap" parameter, which was determined in Ref. 31 in terms of the high-frequency dielectric constant of the semiconductor in question. In the present work ε_g is determined so that the calculation gives the experimental annihilation rates (see below) for delocalized positron states in perfect semiconductors. These parameter values are then used in the defect calculations. The cube root in Eq. (24) follows from the scaling argument between the correlation potential and the contact density (annihilation rate).[32]

After the positron potential is constructed in all space of the perfect lattice, we solve for the positron wave function at $\mathbf{k}=0$ and corresponding to the lowest energy band using the LMTO-ASA method. In the case of a cubic (metal) lattice, where all atomic spheres are equivalent, this calculation corresponds to finding the lowest-energy s function, with a vanishing (logarithmic) derivative at the surface of the sphere. When there is more than one type of sphere, the method gives the distribution of the positron in the different spheres. In order to calculate positron states in lattice defects, we first solve for the whole positron band structure and determine the unperturbed Green's function for the positron. The positron potential is constructed for the perturbed spheres in the defected lattice using the electron density and Coulomb potential from the self-consistent defect calculation. Then the position of a possible bound positron state at the defect is determined by searching for a solution to Eq. (21). If a bound state is found, the corresponding positron density is determined from the perturbed Green's function.

The positron annihilation rate λ depends on the overlap between the positron and electron densities through

$$\lambda=\pi r_0^2c\int d^3r\,|\psi_+(\mathbf{r})|^2n(\mathbf{r})\gamma(n(\mathbf{r})) , \quad (26)$$

where r_0 is the classical electron radius, c the speed of light, $|\psi_+(\mathbf{r})|^2$ the positron density, and γ the short-range enhancement factor. The electron density can be decomposed into a valence (n_v) and a core electron (n_c) part, with the respective enhancement factors γ_v and γ_c. For the core electrons we use the independent-particle annihilation rate with a constant (density-independent) enhancement factor

$$\gamma_c=1.5 . \quad (27)$$

The annihilation rate with valence electrons is associated with the enhancement

$$\gamma_v = 1 + f(n_v, \varepsilon_g)\Delta g(n_v) , \tag{28}$$

where the reduction factor $f(n_v, \varepsilon_g)$ is given by Eq. (25). $\Delta g(n_v)$ describes the density enhancement in the electron gas:[32]

$$\Delta g(n_v) = 1 + \frac{r_s^3 + 10}{6} , \tag{29}$$

where $r_s = (3/4\pi n_v)^{1/3}$ is the usual density parameter in atomic units.

III. RESULTS AND DISCUSSION

A. Comparison with previous positron-state calculations

Before the presentation of our results for Si and GaAs we briefly discuss the effects of the approximations made in the present calculations. The perfect Al fcc lattice and an Al vacancy are used here as examples, because for these there exist several calculations with different methods, making a detailed comparison possible.

The results for perfect Al are collected in Table I. E_{corr} is the electron-positron contribution to the total energy defined as

$$E_{\text{corr}} = \int d^3r \, |\psi_+(\mathbf{r})|^2 V_{\text{corr}}(\mathbf{r}) . \tag{30}$$

E_0 is the electrostatic and kinetic energy contribution, i.e., the so-called zero-point energy. E_0 is given relative to the average electrostatic potential $\overline{V}_{\text{Coulomb}}$ on the surface of the Wigner-Seitz cell and is defined as

$$E_0 = \int d^3r \psi_+^*(\mathbf{r})[-\tfrac{1}{2}\nabla^2 + V_{\text{Coulomb}}(\mathbf{r})]\psi_+(\mathbf{r}) - \overline{V}_{\text{Coulomb}} . \tag{31}$$

Results from three different calculations are shown in Table I. Self-consistent (SC) ASA and non-self-consistent (NSC) ASA refer to calculations which use spherical potentials and densities inside the Al Wigner-Seitz sphere. In SC ASA the self-consistent electron density and Coulomb potential from the LMTO-ASA calculation are used. In NSC ASA the electron density and Coulomb potential are obtained by superimposing free Al atoms and taking the spherical averages. In both cases the spherical positron potential is constructed [Eq. (23)] and the positron wave function is determined by solving the spherical Schrödinger equation with the proper boundary condition. The last row (NSC 3D) shows the results from Ref. 9. They are also obtained using the superposition of free atoms, but the spherical averaging is not made. Instead, the full three-dimensional Schrödinger equation for the positron is solved and all integrals are performed in three dimensions. When the results are compared, it is important to note that all three calculations use the same prescription [Eqs. (23)–(29) with $\varepsilon_g = 0$] for the total positron potential and the annihilation rates.

The results from the two NSC calculations show that the effects due to the approximations in the interstitial regions in the ASA are rather small. On the other hand, the use of the self-consistent electron density raises the positron zero-point energy substantially. This can be understood as follows. When the free atoms form a metal lattice, charge transfer occurs from the ion core regions to the interstitial regions in order to constitute the metallic bonding. The charge transfer lowers the positron potential in the interstitial regions relative to the potential obtained by simple superposition of free atoms. On the other hand, the ion cores are less screened after the charge transfer. The net effect is that the potential sensed by the positron becomes steeper and the "allowed volume" for the positron decreases. This increases the positron zero-point energy, which then has an important bearing on the positron binding energy at lattice defects. The effects due to the charge transfer are seen also in the annihilation rates, i.e., the core contribution reduces when the self-consistent electron density is used instead of the non-self-consistent one. This reduction is compensated by an increase in the valence rate. The positron density has relaxed following the electron density and the net effect in the total annihilation rate is small. As a consequence, all τ_b values are in a good agreement with the experimental[33] value of 166 ps.

Table II presents results for the positron annihilation characteristics in an Al vacancy. Values from the present LMTO-ASA Green's-function calculations and from the three-dimensional calculation[9] using atomic superposition are shown. In the Green's-function calculations the perturbed region contains the vacancy site and its 12 nearest-neighbor Al sites. The positron binding energy to the vacancy is 0.6 eV larger than the value obtained in the old calculation. This reflects the effects due to the self-consistency of the electron structure. The total annihila-

TABLE I. Positron properties in a perfect Al lattice. E_{corr} and E_0 are the correlation and zero-point energy contributions defined in Eqs. (30) and (31), respectively. λ_v and λ_c are the annihilation rates with valence and core electrons, respectively. τ_b is the positron bulk lifetime [$\tau_b = 1/(\lambda_v + \lambda_c)$]. SC ASA and NSC ASA refer to the LMTO-ASA calculations, which use self-consistent and non-self-consistent charge densities, respectively. NSC 3D denotes the three-dimensional calculation in Ref. 9 which uses a non-self-consistent electron density.

Calculation method	E_{corr} (eV)	E_0 (eV)	λ_v (ns^{-1})	λ_c (ns^{-1})	τ_b (ps)
SC ASA	−8.40	5.03	5.63	0.32	168
NSC ASA	−8.41	4.51	5.59	0.44	166
NSC 3D	−8.35	4.41	5.45	0.42	170

TABLE II. Positron properties at an Al vacancy. λ_v and λ_c are the annihilation rates with valence and core electrons, respectively. τ_v and E_b are the positron lifetime and binding energy to the vacancy, respectively. SC ASA refers to the LMTO-ASA Green's-function calculation, which uses a self-consistent electron density. NSC 3D refers to the three-dimensional calculation of Ref. 9, which uses a non-self-consistent electron density. For comparison, the results from two calculations using a supercell-APW approach are also given.

Calculation method	λ_v (ns^{-1})	λ_c (ns^{-1})	τ_v (ps)	E_b (eV)
SC ASA	3.87	0.067	254	2.9
NSC 3D	3.87	0.081	253	2.3
Ref. 25	3.87	0.129	250	2.2
Ref. 32	4.24	0.090	231	3.4

tion rate, on the other hand, is again seen to be insensitive to the charge self-consistency. The feedback effects in the calculation of the total annihilation rate are in fact remarkable in that the difference between the superimposed free-atom and self-consistent densities is considerable. For example, the self-consistent electron density at the center of the vacancy is $0.0018a_0^{-3}$, whereas the corresponding superimposed density is about twice as large, $0.0040a_0^{-3}$.

Table II shows also results from two supercell augmented-plane-wave calculations.[27,34] A comparison with the present results is not straightforward because different methods were used to calculate the total positron potential and the annihilation rates. Moreover, in the calculations of Ref. 27 attempts were made to perform the two-component self-consistency of the electron and positron densities, whereas both densities are non-self-consistent in Ref. 34. However, the comparison shows again the sensitivity of the positron binding energy and the insensitivity of the positron lifetime to the approximations made.

The theoretical values for the positron lifetime at an Al vacancy given in Table II are slightly larger than the experimental value of 240 ps.[33] According to Table II, this result is insensitive to the improvements in the electron structure calculations. On the other hand, in Refs. 11 and 12 it is shown that the positron lifetime is sensitive to the relaxation of ionic positions around the vacancy. This relaxation is omitted in all calculations in Table II. A small inward relaxation of the ions surrounding the vacant site would bring theory and experiment into perfect agreement.

B. Electronic properties of vacancies in Si and GaAs

We have calculated the self-consistent electronic structures for ideal (i.e., lattice relaxations are ignored) vacancies in Si and GaAs. Calculations were performed for different charge states, and in the case of GaAs, vacancies in both sublattices were considered. The perturbed regions consist of the vacancy sphere and four atomic spheres and four interstitial spheres adjacent to the vacancy sphere. We have chosen the sphere radii to be the same for all spheres. The electronic structures were calculated using the spin-compensated density-functional formalism in the local-density approximation for exchange and correlation.[35] Before calculating the unperturbed Green's functions, the too-small band gaps predicted by the local-density approximation were corrected to coincide with the experimental ones (1.12 eV for Si and 1.5 eV for GaAs) by a rigid shift of all conduction bands relative to the valence bands (the so-called "scissors operator"[36]).

The calculated change in the density of states due to the vacancy in Si (V_{Si}) and due to the As (V_{As}) or Ga vacancies (V_{Ga}) in GaAs are shown in Figs. 1–3. These figures correspond to neutral vacancies and only the components belonging to the A_1 and T_2 representations of the five representations of the T_d point group are given. The A_1 and T_2 representations can be thought to arise from the dangling sp^3 bonds, a, b, c, and d, as a totally symmetric $a+b+c+d$ combination (A_1) and as threefold degenerate combinations of the type $a+b-c-d$ (T_2). States belonging to the A_1 and T_2 representations have s character and p character at the vacancy site, respectively. Other representations, involving only back bonds, have a small contribution to the total change in the DOS.

The change in the DOS induced by a vacancy in Si is shown in Fig. 1. The tendency of the repulsive perturbation to shift the states to higher energies is clear. In the case of A_1 states, the two resonances at the middle (bonding combination of s-like states) and at the top (bonding combinations of mainly p-like states) of the valence band compensate the negative regions so that the change in the partial DOS for the valence band integrates to zero. In the T_2-induced DOS the negative antiresonances dom-

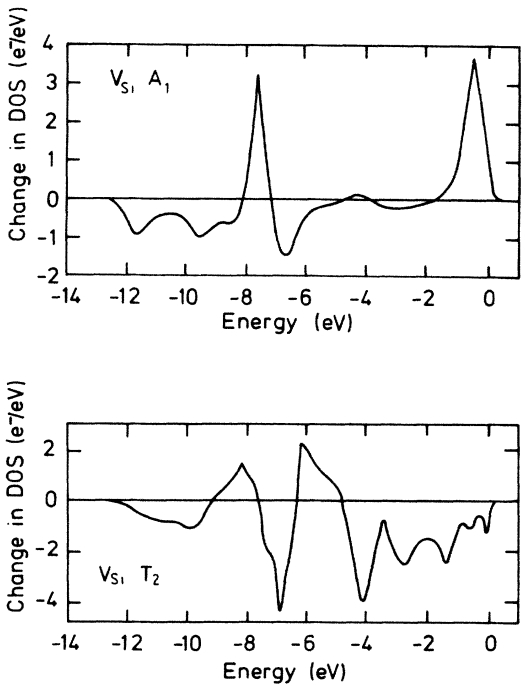

FIG. 1. Changes in the density of states of A_1 and T_2 symmetries induced by a vacancy in Si. The energy zero is the top of valence band.

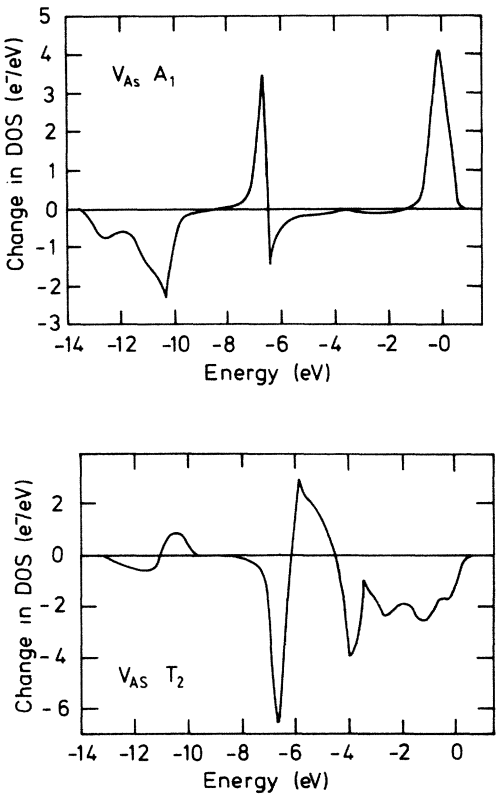

FIG. 2. Changes in the density of states of A_1 and T_2 symmetries induced by an As vacancy in GaAs. The energy zero is the top of valence band.

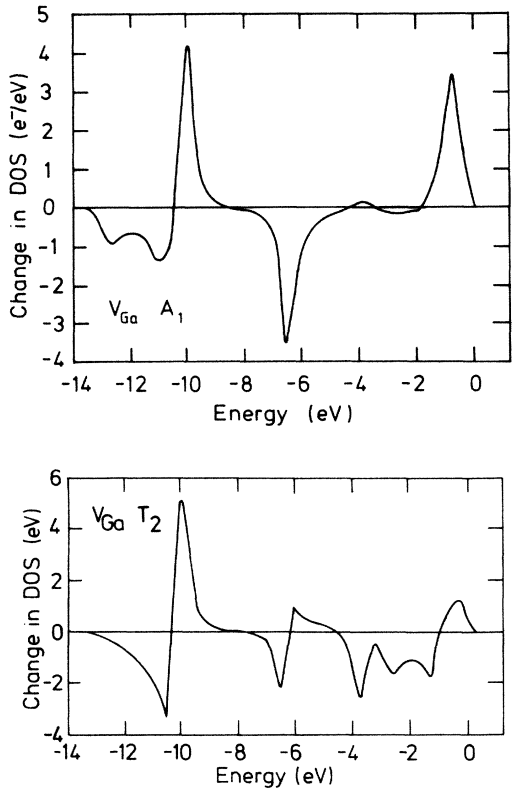

FIG. 3. Changes in the density of states of A_1 and T_2 symmetries induced by a Ga vacancy in GaAs. The energy zero is the top of valence band.

inate so that the integral over the valence band shows a disappearance of six (including the spin degeneracy) electron states. In the creation of a vacancy, four electrons are removed from the valence band. Thus, in the case of a neutral Si vacancy, two electrons have to be filled in states above the valence band. Our calculation for the neutral vacancy gives a T_2-symmetry bound state in the band gap 0.66 eV above the valence-band edge. This sixfold degenerate bound state has in the neutral case one-third occupancy. The change in the DOS and the position of the bound state calculated here by the LMTO-ASA Green's-function method for the ideal Si vacancy is in good agreement with the pseudopotential Green's-function calculations.[37,38] For example, in these calculations the position of the bound state in the gap is 0.7 eV (Ref. 37) or 0.8 eV (Ref. 38). In the real vacancy the position of the bound-state level is strongly affected by the lattice relaxation (a symmetric breathing distortion and/or a symmetry-lowering Jahn-Teller distortion). The relaxation would lower the level from the ideal vacancy position.

The change in the DOS induced by the neutral As and Ga vacancies in GaAs is qualitatively similar to the case of a vacancy in Si, as can be seen by comparing Figs. 2 and 3 with Fig. 1. The lower A_1 resonance for the As vacancy is in fact located in the band gap near the bottom of the valence band and is thus actually a bound state. In Fig. 2 it has a finite width because we have made the plot for the complex energy path slightly below the real axis. Whether this structure is a bound state or a resonance in the band region is not important for our calculations which use the complex energy integration. The same is true for the A_1 and T_2 bound states (or resonances) at the bottom (~ -10 eV) of the lower energy gap in the case of the Ga vacancy. As in the case of the Si vacancy, the total number of induced A_1 states in the valence bands is zero for both As and Ga vacancies. The repulsive potential due to the As or Ga vacancy pushes a sixfold degenerate T_2 state out of the valence band. For the neutral As vacancy it is placed 1.13 eV above the top of the valence band and it is occupied by one electron, because the number of removed valence electrons is 5. For the neutral Ga vacancy it is situated 0.06 eV above the valence-band edge and it is filled with three electrons, because three valence electrons are removed when the Ga vacancy is created. Lattice relaxation would lower these levels and the bound state of the Ga vacancy might appear as a resonance in the valence band, and only the As-vacancy state would remain as a deep level.

Our results for the changes in the DOS and the bound-state positions agree well with the pseudopotential-Green's-function calculations by Bachelet *et al.*[39] For example, they found the bound-state levels at 0.06 and 1.08 eV above the top of the valence band for the Ga and As vacancies, respectively. The large-cluster recursion ap-

proach applied by Lin-Chung and Reinecke[40] gives the bound-state level in the As vacancy at 1.21 eV, which is in good agreement with our results. However, their corresponding value for the Ga vacancy, 0.44 eV above the valence band, is considerably larger than ours.

We have also considered charged vacancies in Si and GaAs. In these calculations the effects of the long-range Coulomb potential were taken into account by shifting the electron potential in the perturbed region by the amount of $q \times 0.1$ eV, where q is the net charge of the defect.[41]

The energy levels of the T_2 bound states induced by the vacancies in Si and GaAs are collected in Table III. The spatial localization of the bound state given in Table III is obtained by integrating the bound electron density over the perturbed region (the vacancy sphere and four atom and four interstitial spheres). These quantities are shown for different charge states. The bound states are seen to be rather delocalized, only about 30—40 % of the bound electron resides in the perturbed region. Adding more electrons to the bound level raises the level of energy, but the change in the localization is rather small. Although the bound states are rather delocalized, the total charge inside the perturbed region around a neutral vacancy is close to its asymptotic value. For example, in the case of the neutral Si vacancy there is a total charge transfer of only 0.07 electrons out from the perturbed region, although 1.28 electrons of the two bound electrons are outside the perturbed region. This means that the electrons belonging to the bound states, to the resonances, and to the antiresonances can screen each other very efficiently. As a consequence, the potential perturbation due to a defect is well localized. The power of the Green's-function method is based on this localization, because only the rather localized perturbation in the potential enters the Dyson's equation, while the wave functions may extend beyond the perturbed region. On the other hand, in the popular cluster methods the size of the cluster must be so large that the effect of the cluster boundaries on the wave functions near the defect is small. This means that most of the bound state should be confined inside the cluster. The too-small size seems to be the most severe source of errors in the cluster calculations.

TABLE III. Energies and spatial localization of the bound electronic (T_2) states due to ideal vacancies in Si and GaAs. Energies are measured from the top of the valence band. The relative localization gives the fraction of the bound electron contained in the perturbed region consisting of the vacancy sphere and the adjacent four atomic and four interstitial spheres.

Vacancy type	E_b (eV)	Localization (%)	Number of bound electrons
V_{Si}^{0}	0.66	41	2
V_{Si}^{2-}	0.93	39	4
V_{As}^{0}	1.13	30	1
V_{As}^{-}	1.22	29	2
V_{As}^{2-}	1.31	28	3
V_{Ga}^{0}	0.06	34	3
V_{Ga}^{2-}	0.23	39	5

C. Positron states and annihilation characteristics in Si and GaAs

The parameter ε_g describing the effect of the band gap on the electron-positron correlation, appearing in the formulas for the positron correlation potential [Eq. (24)] and annihilation rate [Eq. (28)] via the reduction factor [Eq. (25)] was determined for Si and GaAs so that the perfect-lattice calculations reproduce the experimental positron lifetime of 221 ps for bulk Si (Ref. 42) and 235 ps for bulk GaAs (Ref. 6). The same value, $\varepsilon_g = 0.2$, was found to fulfill this requirement for both semiconductors. The experimental bulk lifetime of 220 ps for GaAs suggested in Ref. 5 cannot be reached by adjusting the ε_g parameter. Even the metal limit, i.e., $\varepsilon_g = 0$, gives a longer lifetime than 220 ps.

The resulting positron distributions and the core and valence annihilation rates in different types of spheres in perfect Si and GaAs lattices are shown in Table IV. The distribution is normalized so that the sum over all different types of spheres gives one positron. In both semiconductors about 75% of the positron density is in the interstitial spheres and 25% in the atom spheres. No prominent preference (a larger affinity) for either of the elements in GaAs can be seen (a larger affinity to As atoms was suggested in Ref. 5). Both in Si and GaAs about 55% of the annihilation takes place in the interstitial spheres. The core annihilation rate is small in comparison to the valence rate: it is only 2% of the total annihilation rate in Si and 7% in GaAs.

We used the self-consistent electron structures of ideal Si and GaAs vacancies to calculate the vacancy-induced perturbation in the positron potential. Bound positron states at vacancies were then searched for below the perfect-lattice positron bands by determining the solutions to Eq. (21). For all vacancies studied in this work, one A_1-type bound state was found. Table V lists the positron binding energies (i.e., the difference between the lowest $\mathbf{k}=0$ energy level in the perfect lattice and the energy eigenvalue for the bound state) to vacancies in Si and to Ga vacancies or As vacancies in GaAs for different charge states. The degree of localization of the positron state into the perturbed region is also shown in Table V. The binding energies vary between 0.5—1.7 eV and they are thus somewhat smaller than the binding energies found for positrons at metal vacancies (see, e.g., Table II). This is because the more open structure lowers the perfect-lattice zero-point energy in the semiconductors relative to that in the close-packed metals. It is interesting to note that the binding energy increases nearly linearly as a function of the number of bound electrons in the vacancy. Moreover, this dependence is nearly the same for both kinds of vacancies in GaAs and even between Si and GaAs.

The fraction of the bound positron in the perturbed region is about 70%. This is considerably more than the corresponding localization of $\sim 30\%$ found for bound electrons in the band gap, but it is less than the 100% localization of a positron at the Al vacancy (Table II). Thus

TABLE IV. Positron distributions and annihilation rates in perfect Si and GaAs lattices. The sum of distribution over the different spheres is normalized to give one positron. The sum of annihilation rates over the different spheres gives the total annihilation rate in the bulk lattice. E refers to the interstitial sphere in the Si lattice. E_1 and E_2 denote interstitial spheres in GaAs adjacent to Ga and As spheres, respectively. λ_v and λ_c are the positron annihilation rates with valence and core electrons, respectively. τ_b is the experimental bulk lifetime used to fit the parameter ε_g in Eqs. (24) and (28).

	Sphere	Distribution (e^+/sphere)	λ_v (ns^{-1})	λ_c (ns^{-1})	τ_b (ps)
Si					
	Si	0.248	1.93	0.10	221[a]
	E	0.753	2.51	—	
	Total	1.000	4.44	0.10	
GaAs					
	Ga	0.119	0.70	0.18	
	As	0.123	0.98	0.10	235[b]
	E_1	0.388	1.21		
	E_2	0.370	1.09	—	
	Total	1.000	3.97	0.28	

[a]Reference 42.
[b]Reference 6.

in these semiconductors a positron spills out, to some extent, from the immediate vicinity of the vacancy to the rather open interstitial regions.

The valence and core annihilation rates and the resulting lifetimes for positrons trapped by different types of vacancies are given in Table V. In the calculations the annihilation rate outside the perturbed region is approximated to be the same as in the atom and interstitial spheres adjacent to the vacancy. This is not a severe approximation: for example, if the annihilation rate corresponding to the perfect crystal is used for the contribution from the unperturbed region, the lifetime of the trapped positron changes by less than 1%. According to Table V the positron lifetime is rather insensitive to the charge state of the vacancy, although the positron binding energy changes considerably. This reflects again the ability of the positron to follow the electron charge transfer. In this case, the introduction of a relatively delocalized bound electron locally changes the electron density only slightly relative to the total electron density. Also, the screening effects work in this direction. However, an evident trend is a small increase in the lifetime as a function of the number of bound electrons. The increase in the lifetime is a consequence of the higher localization of the positron wave function to the perturbed region where the electron density and thus the annihilation rate are smaller than those farther away from the vacancy. However, the predicted changes in the positron lifetime due to changes in the charge of the state are small and hard to distinguish in the experimental positron lifetime spectra.

The calculated lifetime of 259 ps for the positron trapped at the Si vacancy agrees rather well with the generally accepted experimental value of 266 ps.[42–44] The slightly smaller theoretical number could be brought into

TABLE V. Properties of positrons trapped at vacancies in Si and GaAs. λ_v and λ_c are the positron annihilation rates with valence and core electrons, respectively. τ_v and E_b are the positron lifetime and binding energy at the vacancy, respectively. The relative localization gives the fraction of the bound positron contained in the perturbed region.

Vacancy type	λ_v (ns^{-1})	λ_c (ns^{-1})	τ_v (ps)	E_b (eV)	Localization (%)
V_{Si}^{2+}	3.87	0.069	254	0.5	63
V_{Si}^{0}	3.79	0.063	259	1.0	71
V_{Si}^{2-}	3.77	0.057	261	1.6	76
V_{As}^{+}	3.36	0.26	276	0.6	65
V_{As}^{0}	3.34	0.25	279	0.8	68
V_{As}^{-}	3.32	0.25	280	1.0	71
V_{As}^{2-}	3.30	0.24	282	1.2	73
V_{Ga}^{0}	3.59	0.15	267	1.3	73
V_{Ga}^{2-}	3.55	0.15	270	1.7	76

perfect agreement with the experimental one by allowing a small outward relaxation of the nearest atoms of the vacancy. The outward relaxation decreases positron-electron overlap and thus increases the positron lifetime. Indeed, it is theoretically[45] predicted that the vacancy-site—nearest-neighbor distance is about 5% larger than the bond length in the perfect lattice. In our present self-consistent calculations this relaxation has been omitted. In the model[9] based on the atomic superposition and on the fully three-dimensional solution of the positron wave function, it is easy to take the lattice relaxation into account, and from this kind of calculation[11,12] it is concluded that the lattice relaxation is an important factor affecting the lifetime value. As a matter of fact, the lattice relaxation seems to be more important for the lifetime value than the self-consistency of the electron density. It is also gratifying to note that for metal vacancies, for which an inward relaxation is expected, our present model (see Table II for Al) and the previous calculations[9,11] always give longer positron lifetime values than the measured ones.

The calculated positron lifetimes for As vacancies in GaAs are slightly shorter than the lifetime component of 290—300 ps seen in the experiment with undoped GaAs.[5,6] Taking into account the effects of the possible lattice relaxation, our calculation supports the assignment[6] of this lifetime component to the As vacancy. Hautojärvi *et al.*[7] have also seen a shorter lifetime component of 260—280 ps in GaAs samples electron irradiated at low temperatures. This component was connected with the Ga vacancy. Also, according to our calculations (Table V), the positron lifetime for the Ga vacancy is shorter than for the As vacancy.

According to the experiments it is evident that positive vacancies cannot trap positrons. For example, *p*-type boron-doped Si has not revealed positron trapping at defects after electron irradiation.[42] The irradiation creates vacancies, but when the material remains *p* type, the Fermi level is below the defect-induced bound states in the band gap and the defects are positively charged. It is then natural to assume that the repulsive Coulomb interaction prohibits positron trapping and no long defect component in the positron lifetime spectra can be seen. Furthermore, positron lifetime measurements have shown that the average lifetime in *n*-type GaAs is substantially longer than in *p*-type or semi-insulating GaAs.[6] The As vacancy is a donor-type defect with deep levels in the upper half of the band gap (Table IV). In *p*-type or in semi-insulating GaAs the Fermi level is below these donor levels and the As vacancy is positively charged. If trapping at positive As vacancies is prohibited, the positron lifetime spectra in *p*-type or semi-insulating GaAs do not contain the long lifetime component of 290—300 ps and the average lifetime decreases. The inability of positively charged vacancies to trap a positron is necessary also in the above-mentioned identification of Ga vacancies from the lifetime measurements.[7] In this case electron irradiation creates a large number of Ga and As vacancies. The acceptor-type levels of the Ga vacancy are first occupied leaving the As vacancies positively charged. In this process originally *n*-type GaAs becomes semi-insulating. When the positively charged As vacancies are not able to trap positrons, the measured long-lifetime component has to be connected with Ga vacancies.

However, according to our calculations (Table V), positive vacancies can bind positrons. This result can be qualitatively explained as follows. The case of one positron and one hole bound to a vacancy is analogous to the doubly negatively charged vacancy. In the latter case the introduction of the second electron raises the bound-state level by 0.1—0.2 eV (Table V). In the former case the introduction of the hole into the vacancy raises the positron bound-state level by ~ 0.2 eV, consistently with the electron case. The introduction of one hole in the vacancy does not destroy the bound positron state. On the other hand, the presence of the hole creates a long-range repulsive Coulomb potential for the positron, which results in a wide wall with a height of around 0.1 eV.[40] The thermal energy of a delocalized (free) positron is about one order of magnitude smaller. Thus the free positron is strongly affected by this potential wall and its wave function is strongly reduced at the vicinity of the positively charged defect. The trapping rate of positrons is, via the Fermi golden rule, proportional to the matrix element between the initial free state and the final trapped state. Due to the small overlap of these two states this matrix element can become very small. Thus it is most conceivable that, in agreement with experimental conclusions, positive vacancies do not trap positrons; while positively charged vacancies *do* support bound states, the trapping rate into them is negligible.

The question of trapping mechanisms and their temperature dependence in semiconductors is most interesting and will be discussed separately.[46] For example, in many cases the binding energy to a vacancy is smaller than the band gap (Table V). This implies that the electron-hole pair excitation mechanism, dominating in metals, is forbidden. On the other hand, the vacancy defects can have a large effect on the density of final electron-hole states and simple estimates of the trapping rates are not very reliable. The important question is if (and how) the trapping rate in semiconductors can be (as suggested by experiments[47] similar in magnitude to the ones in metals. The phonon mechanism, either as a multiphonon or a cascade process, seems to give much lower values for the trapping rate.[46]

IV. CONCLUSIONS

This paper reports calculations of the electronic structure of point defects in Si and GaAs using state-of-the-art LMTO-ASA Green's-function techniques. The results are applied in a study of positron annihilation in these semiconductors to both the bulk and vacancy bound states, with the aim of making feasible definitive interpretations in positron defect spectroscopy. The main conclusions are the following.

(1) The *ab initio* results for the electronic structure and positron annihilation characteristics agree well with experiment for bulk materials and for defects where an unambiguous assignment is possible.

(2) The positron binding energy to a vacancy-type defect is small, in many cases smaller than the band gap.

(3) The effect of the charge state of the vacancy on positron parameters is small. The experimentally seen changes could be due to changes in the trapping rate.

(4) A positively charged vacancy can support a bound positron state, but the trapping rate into such a state is argued to be strongly reduced.

(5) The calculations provide benchmarks for more approximate approaches (e.g., non-self-consistent electronic structure), which presently are necessary for more complicated defects with low symmetry. The relative insensitivity of the annihilation rates to reasonable approximations in the electronic structure part of the calculation is encouraging for the development of such techniques.

ACKNOWLEDGMENTS

Discussions with O. K. Andersen, F. Beeler, C. Corbel, and P. Hautojärvi are gratefully acknowledged.

*Permanent address: Helsinki University of Technology, Laboratory of Physics, SF-02150 Espoo, Finland.

[1]*Proceedings of the 13th International Conference on Defects in Semiconductors, Coronado 1984,* edited by L. C. Kimerling and J. M. Parsey (The Metallurgical Society of AIME, New York, 1984).

[2]D. Ponds and J. C. Bourgoin, J. Phys. C **18**, 3839 (1985).

[3]*Positrons in Solids,* Vol. 12 of *Topics in Current Physics,* edited by P. Hautojärvi (Springer, Heidelberg, 1979).

[4]*Positron Solid State Physics,* proceedings of the Enrico Fermi International School of Physics, Course LXXXIII, edited by W. Brandt and A. Dupasquier (North-Holland, Amsterdam, 1983).

[5]S. Dannefaer, B. Hogg, and D. Kerr, Phys. Rev. B **30**, 3355 (1984).

[6]G. Dlubek, O. Brummer, F. Plazaola, and P. Hautojärvi, J. Phys. C **19**, 331 (1986).

[7]P. Hautojärvi, P. Moser, M. Stucky, and C. Corbel, Appl. Phys. Lett. **48**, 809 (1986).

[8]M. Stucky, R. Paulin, B. Geffroy, C. Corbel, and J. Suskij, in *Proceedings of the 7th International Conference on Positron Annihilation, New Delhi 1985,* edited by P. C. Jain, R. M. Singru, and K. P. Gopinathan (World Scientific, Singapore, 1985).

[9]M. J. Puska and R. M. Nieminen, J. Phys. F **13**, 333 (1983).

[10]M. J. Puska and R. M. Nieminen, J. Phys. F **12**, L211 (1982).

[11]H. E. Hansen, R. M. Nieminen, and M. J. Puska, J. Phys. F **14**, 1299 (1984).

[12]C. Corbel, M. Puska, and R. M. Nieminen, Radiat. Eff. **79**, 305 (1983).

[13]P. Hautojärvi, H. Huomo, M. Puska, and A. Vehanen, Phys. Rev. B **32**, 4326 (1985).

[14]O. K. Andersen, Phys. Rev. B **12**, 3060 (1975).

[15]H. C. Skriver, *The LMTO Method* (Springer, New York, 1984).

[16]O. K. Andersen, O. Jepsen, and D. Glötzel, in *Highlights of Condensed-Matter Theory,* proceedings of the Enrico Fermi International School of Physics, Course LXXXIX, edited by F. Bassani, F. Fumi, and M. P. Tosi (North-Holland, Amsterdam, 1985).

[17]O. Gunnarsson, O. Jepsen, and O. K. Andersen, Phys. Rev. B **27**, 7144 (1983).

[18]D. Glötzel, B. Segall, and O. K. Andersen, Solid State Commun. **36**, 403 (1980).

[19]A. K. Singh and T. Jarlborg, J. Phys. F **15**, 727 (1985).

[20]F. Beeler, M. Scheffler, O. Jepsen, and O. Gunnarsson, Phys. Rev. Lett. **54**, 2525 (1985).

[21]F. Beeler, O. K. Andersen, and M. Scheffler, Phys. Rev. Lett. **55**, 1498 (1985).

[22]O. K. Andersen, and O. Jepsen, Phys. Rev. Lett. **53**, 2571 (1984).

[23]O. Jepsen and O. K. Andersen, Solid State Commun. **9**, 1763 (1971).

[24]C. Koenig, J. Phys. C **3**, 1497 (1973); H. Dreysse and R. Riedinger, J. Phys. (Paris) **42**, 437 (1981); R. Zeller, J. Deutz, and P. H. Dederichs, Solid State Commun. **44**, 993 (1982).

[25]*Theory of the Inhomogeneous Electron Gas,* edited by S. Lundqvist and N. H. March (Plenum, New York, 1983).

[26]R. M. Nieminen, in Ref. 4, p. 359.

[27]B. Chakraborty and R. W. Siegel, Phys. Rev. B **27**, 4535 (1983).

[28]R. M. Nieminen, E. Boronski, and L. J. Lantto, Phys. Rev. B **32**, 1377 (1985).

[29]E. Boronski and R. M. Nieminen Phys. Rev. B (to be published).

[30]J. Arponen and E. Pajanne, Ann. Phys. (N.Y.) **121**, 343 (1979); J. Phys. F **9**, 2359 (1979).

[31]W. Brandt and J. Reinheimer, Phys. Rev. B **2**, 3104 (1970).

[32]W. Brandt and J. Reinheimer, Phys. Lett. **35A**, 109 (1971).

[33]M. J. Fluss, L. C. Smedskjaer, M. K. Chason, D. G. Legnini, and R. W. Siegel, Phys. Rev. B **17**, 3444 (1978).

[34]R. P. Gupta and R. W. Siegel, Phys. Rev. B **22**, 4572 (1980).

[35]U. von Barth and L. Hedin, J. Phys. C **5**, 1629 (1972).

[36]G. Baraff and M. Schlüter, Phys. Rev. B **30**, 3460 (1984).

[37]G. A. Baraff and M. Schlüter, Phys. Rev. Lett. **41**, 892 (1978); Phys. Rev. B **19**, 4965 (1979).

[38]J. Bernholc, N. O. Lipari, and S. T. Pantelides, Phys. Rev. Lett. **41**, 895 (1978); Phys. Rev. B **21**, 3545 (1980).

[39]G. B. Bachelet, M. Schlüter, and G. A. Baraff, Phys. Rev. B **27**, 2545 (1983).

[40]P. J. Lin-Chung and T. L. Reinecke, Phys. Rev. B **27**, 1101 (1983).

[41]C. O. Rodriquez, S. Brand, and M. Jaros, J. Phys. C **13**, L333 (1980).

[42]W. Fuhs, V. Holzhauer, S. Mantl, F. W. Richter, and R. Sturm, Phys. Status Solidi B **89**, 69 (1978).

[43]S. Dannefaer, G. A. Dean, D. P. Kerr, and B. G. Hogg, Phys. Rev. B **14**, 2709 (1976).

[44]S. Dannefaer, S. Kupca, B. G. Hogg, and D. P. Kerr, Phys. Rev. B **22**, 6135 (1980).

[45]M. Scheffler, J. P. Vigneron, and G. P. Bachelet, Phys. Rev. B **31**, 6541 (1985).

[46]R. M. Nieminen (unpublished).

[47]Shimotomai, Y. Ohgino, H. Fukushima, Y. Nagayasu, T. Mihara, K. Inonue, and M. Doyama, in *Defects and Radiation Effects in Semiconductors 1980,* Vol. 59 of *Institute of Physics Conference Series* (The Institute of Physics, Bristol, 1981), p. 241.